Supporting Information

Carbon Aerogel Evolution: Allotrope, Graphene-Inspired, and 3D-Printed Aerogels

Swetha Chandrasekaran, Patrick G. Campbell, Theodore F. Baumann, Marcus A. Worsley*

Lawrence Livermore National Laboratory, 7000 East Ave, Livermore, California, United States 94551

*corresponding author: worsley1@llnl.gov

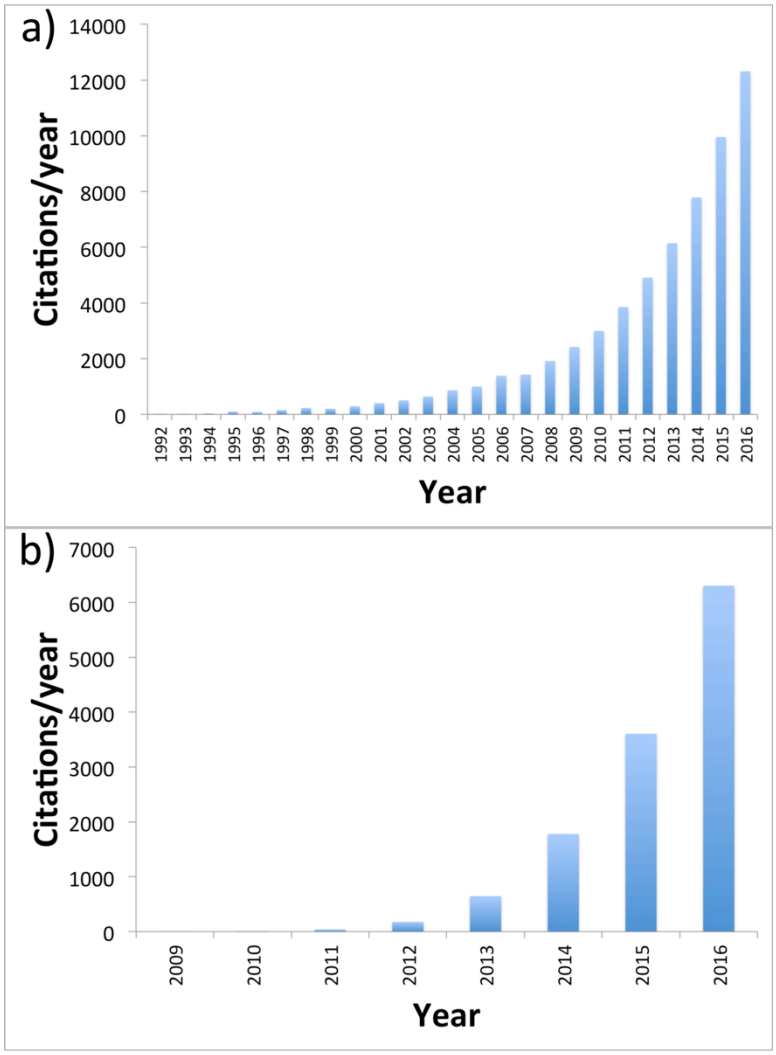

Figure S1. Citations per year for a) carbon aerogel and b) graphene aerogel publications.

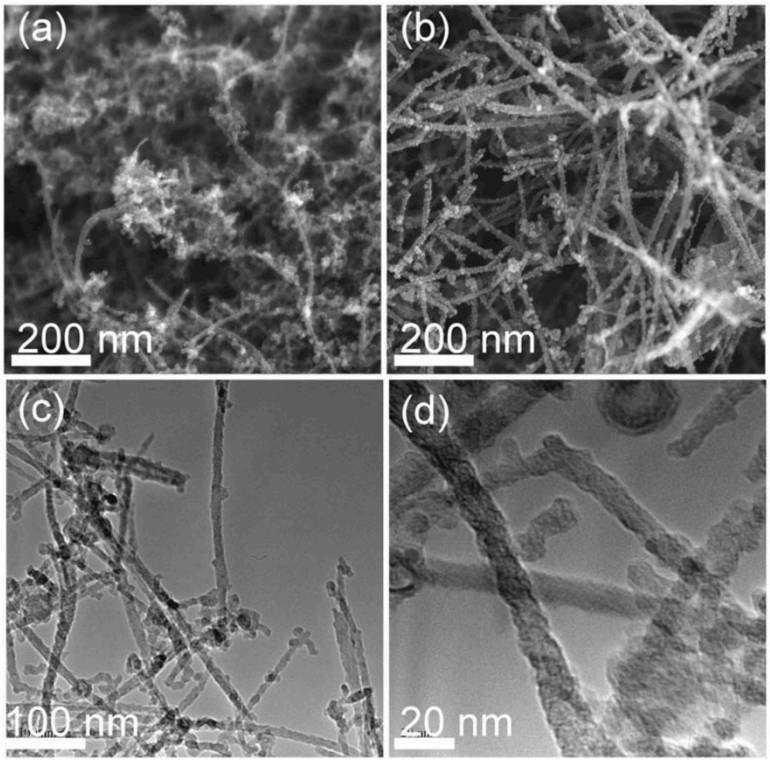

Figure S2. SEM images of CNT foams containing a) 30 wt% and b) 55 wt% CNTs and TEM images c) and d) at different magnifications of a foam containing 30 wt % CNT. Reproduced by permission from Ref. 43 (American Institute of Physics).

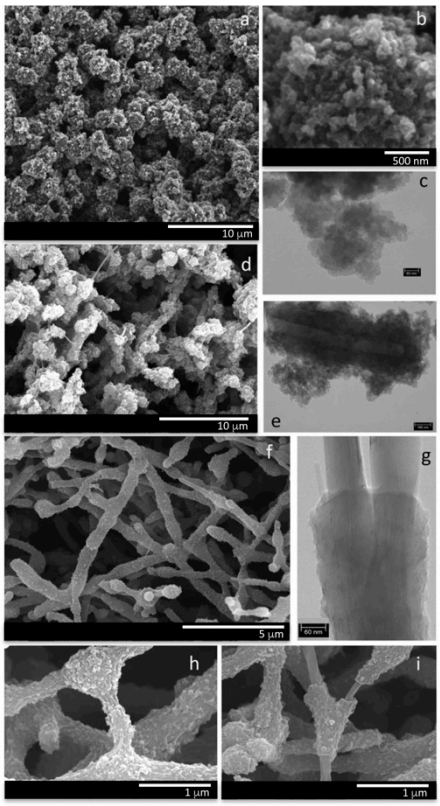

Figure S3. SEM micrographs of a,b) CA, d) CA with 13 wt% CNT, and f,h,i) CA with 41 wt% CNT. TEM micrographs of the colloidal carbon corresponding to c) CA and CA with 13 wt% CNT, and e,g) of the fibrillar carbon corresponding to CA with 13 and 41 wt% CNT. Reproduced by permission from Ref. 48 (Wiley and Sons).

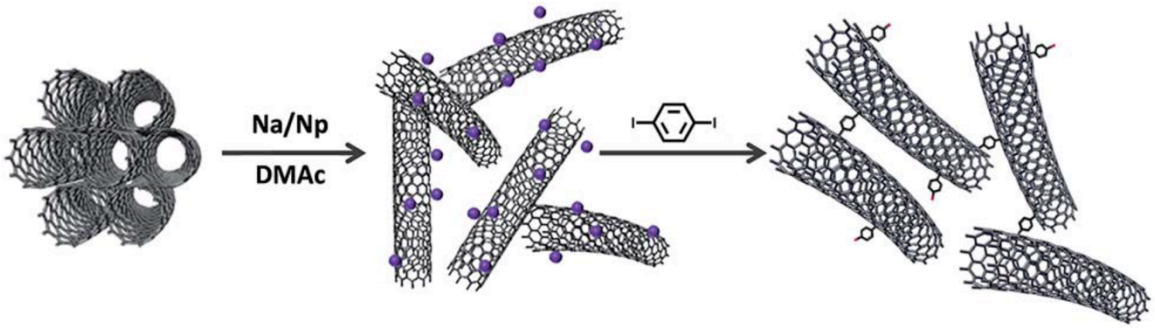

Figure S4. Representation of reaction scheme for crosslinking CNTs. Reproduced by permission from Ref. 50 (Royal Society of Chemistry).

.

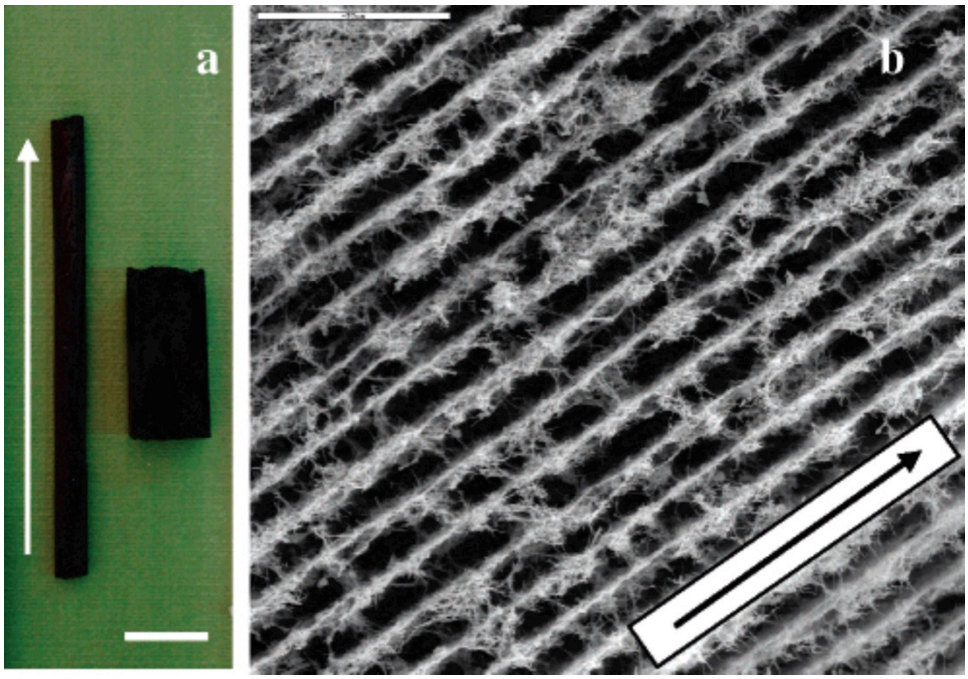

Figure S5. Picture of MWCNT/CHI monoliths with different shapes and sizes resulting from the ISISA processing of MWCNT/CHI suspensions placed in different disposable containers; an insulin syringe (left) and a polystyrene cuvette (right) (a) (bar is 1 cm). SEM micrograph of the longitudinal section of a MWCNT/CHI monolith (b) (bar is 50 mm). The MWCNT content of every monolith shown in the figure is 85 wt %. Arrows indicate the direction of freezing. Reproduced by permission from Ref. 53 (American Chemical Society).

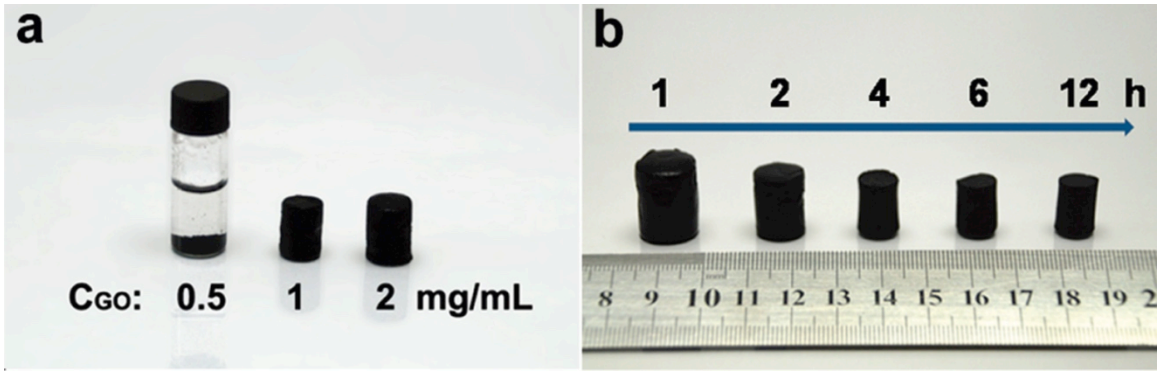

Figure S6. (a) Photographs of the products prepared by hydrothermal reduction of GO dispersions with different GO concentrations at 180°C for 12 h; (b) photographs of the products prepared by hydrothermal reduction of 2 mg mL^{-1} of GO at 180°C for different times. Reproduced by permission Ref. 71 (American Chemical Society).

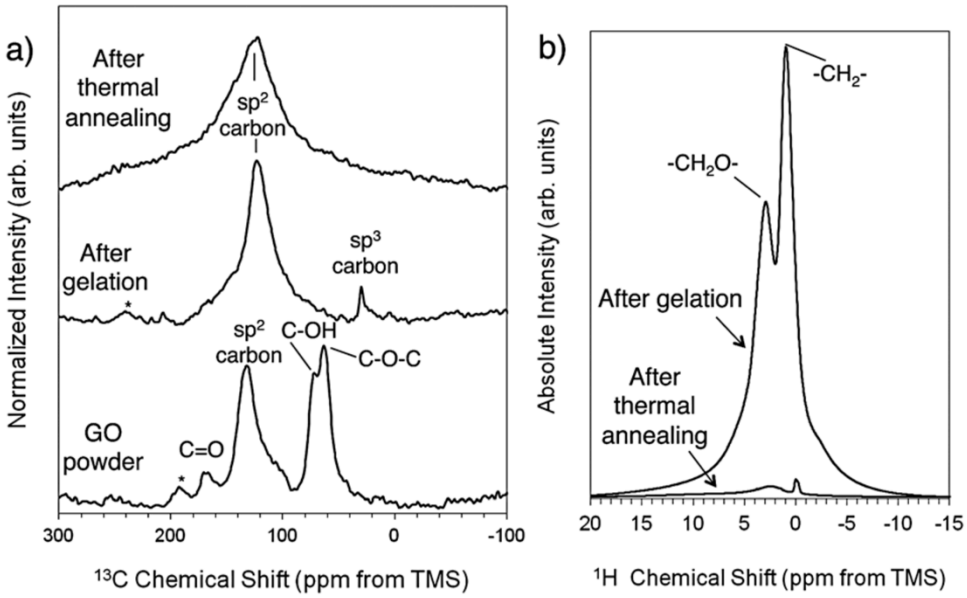

Figure S7. (a) ^{13}C and (b) ^{1}H NMR spectra for GO powder, GO after initial gelation, and GA. Reproduced by permission from Ref. 83 (Royal Society of Chemistry).

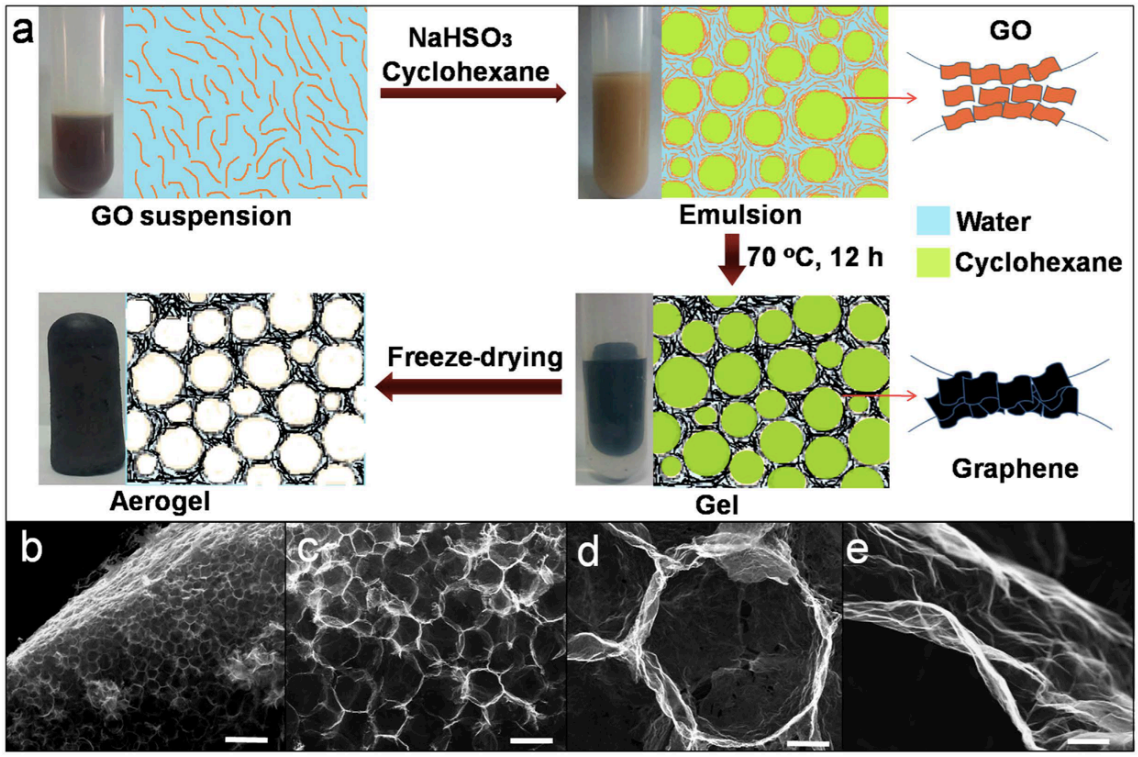

Figure S8. (a) Scheme illustrating the synthesis process of GA from the assembly of GO at oil-water interface and the subsequent chemical reduction. (b) Whole view of the GA derived from the emulsion with GO concentration of 2.00 mg/mL, revealing that the bulk of aerogel is entirely composed of cellular-like pores. (c) The image shows the closely linked pores with polyhedral morphology. (d) A hexagonal pore shares the boundary with other six adjacent pores, ensuring the firm bridge of the

connection. (e) The ultrathin and wrinkled wall. Reproduced by permission from Ref. 93 (Nature Publishing Group).

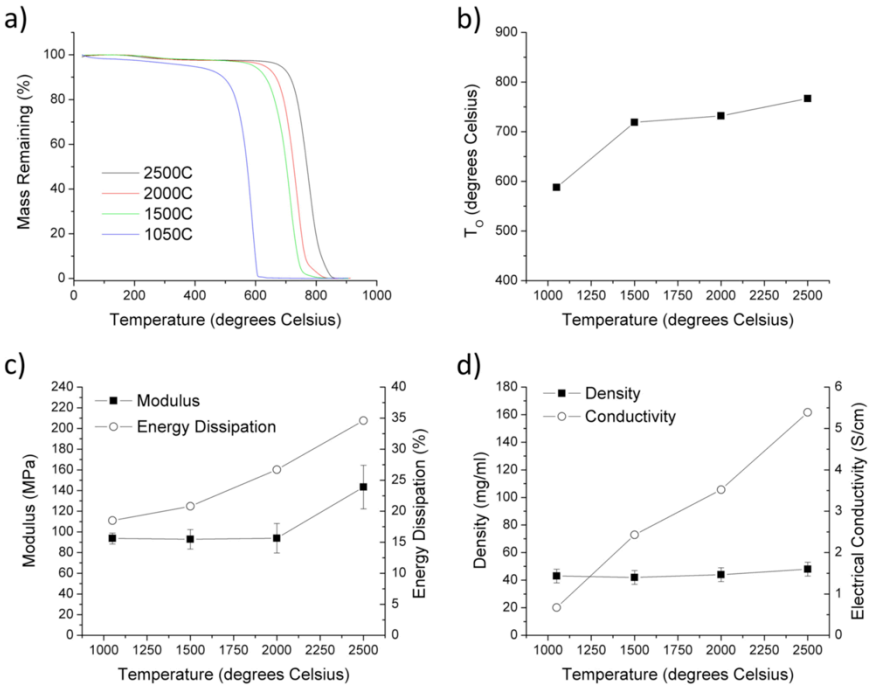

Figure S9. (a) TGA curves for the GA treated at 1050, 1500, 2000, and 2500°C. (b) Oxidation temperature, T_O, of GA vs annealing temperature. (c) Young's modulus and energy loss for GA vs annealing temperature. (d) Bulk density and electrical conductivity of GA vs annealing temperature. Reproduced by permission from Ref. 100 (American Chemical Society).

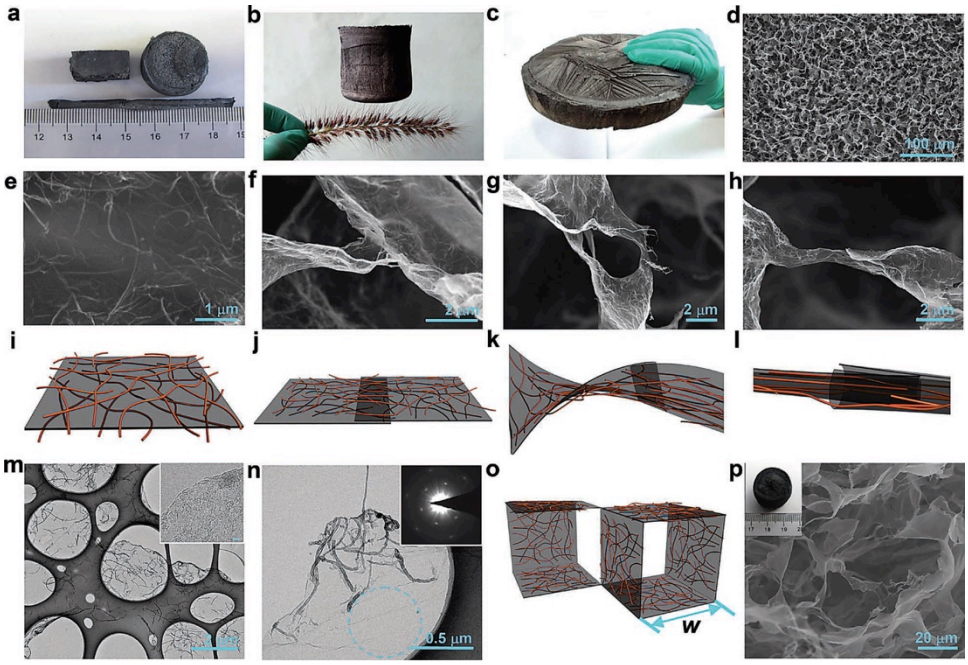

Figure S10. Macroscopic and Microscopic structures of CNT/GAs. (a) Digital photograph of CNT/GAs with diverse shapes. (b) A 100 cm^3 CNT/GA cylinder standing on a flower-like dog's tail (Setaira viridis (L.) Beauv). (c) A ~ 1000 cm^3 CNT/GA cylinder (21 cm in diameter and 3 cm in thickness). (d-e) Microscopically porous architecture of a CNT/GA at different magnifications, showing CNT-coated graphene cell walls. (f-h) SEM images of different interconnections for CNTs-coated graphene (graphene@CNTs) cell walls: overlapping (f), twisting (g), and wrapping (h). (i) Cartoon of a flattened CNT-coated graphene cell wall. (j-l) Cartoon models corresponding to the three interconnection styles shown in (f-g) respectively. The gray lamellar, orange wires and brown wires represent the graphene sheet, CNTs coated on the top and CNTs coated on the back of the graphene sheet, respectively. (m,n) TEM images of CNT-coated graphene cell walls, the HRTEM image of a cell wall edge (inset in (m), scale bar is 2 nm) and the SAED patterns (inset in (n)) taken at the labeled area. (o) Schematic illustration of idealized building cells of our CNT/GA made by synergistic assembly of graphene and CNTs. (p) SEM image and photograph (inset in (p)) of the lightest neat graphene aerogel (ρ = 0.16 mg cm^{-3} , i.e., 1.38 mg in 8.6 cm^3). Reproduced by permission from Ref. 103 (Wiley and Sons).

.

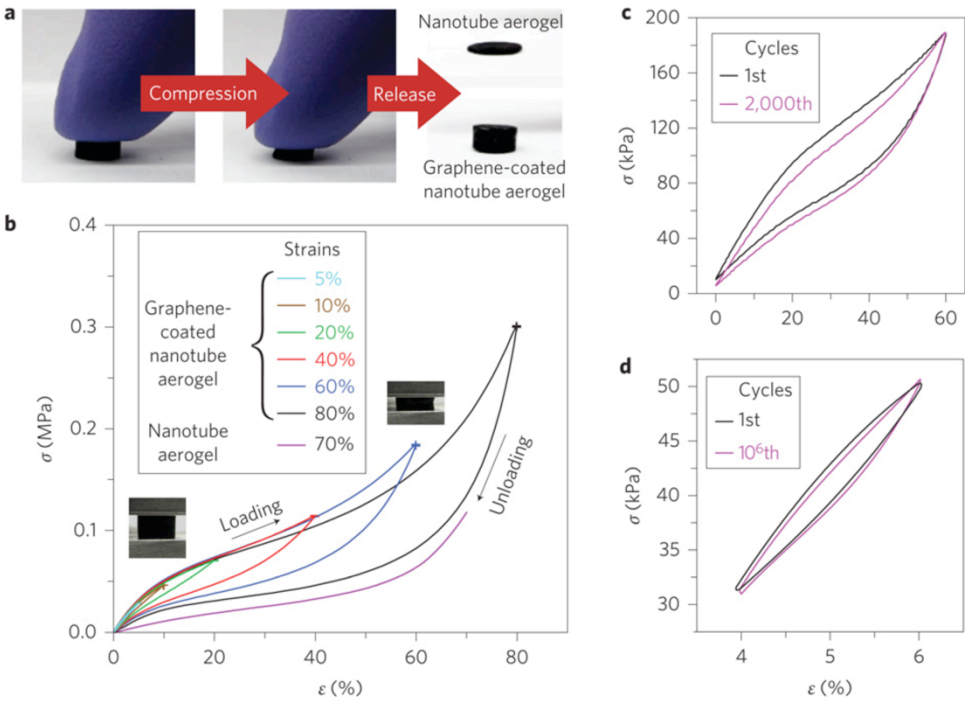

Figure S11. **a** Macroscopic visualization, showing that nanotube aerogels collapse and graphene-coated aerogels recover their original shape after compression by ≥90%. **b**, σ versus ε curves for nanotube aerogels along the loading direction and for graphene-coated aerogels during loading–unloading cycles. The hysteresis increases at larger ε for the graphene-coated aerogels. Insets: photographs of aerogels after graphene coating at ε = 0% (left) and 60% (right). **c**,**d**, Fatigue resistance of graphene-coated nanotube aerogel at 60% strain, 1 Hz, for the 1st and 2,000th cycles (**c**) and at 2% strain, 100 Hz, for the 1st and 10^6th cycles (**d**). Reproduced by permission from Ref. 39 (Nature Publishing Group).

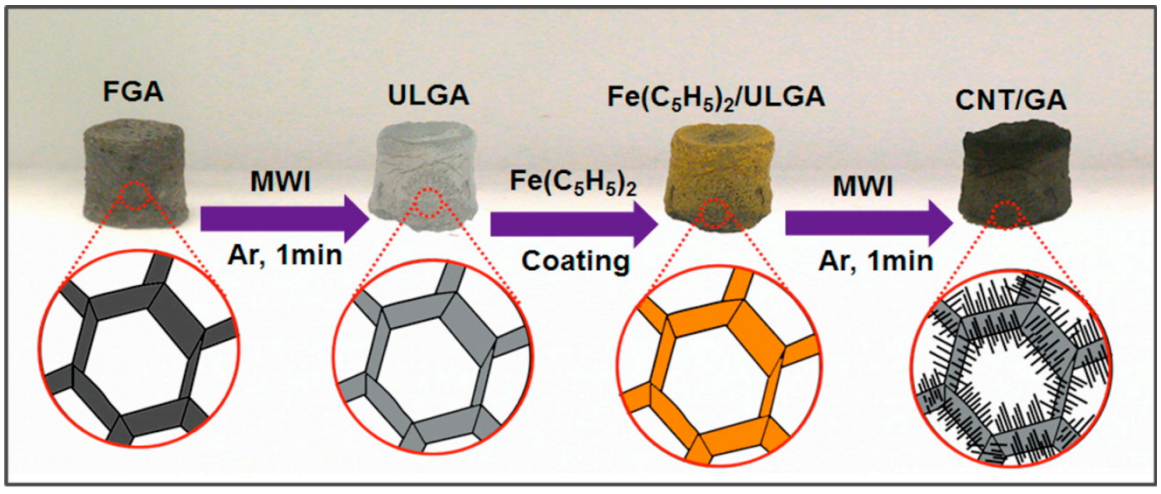

Figure S12. Fabrication scheme for CNT/GA via microwave irradiation (MWI). Reproduced by permission from Ref. 106 (American Chemical Society).

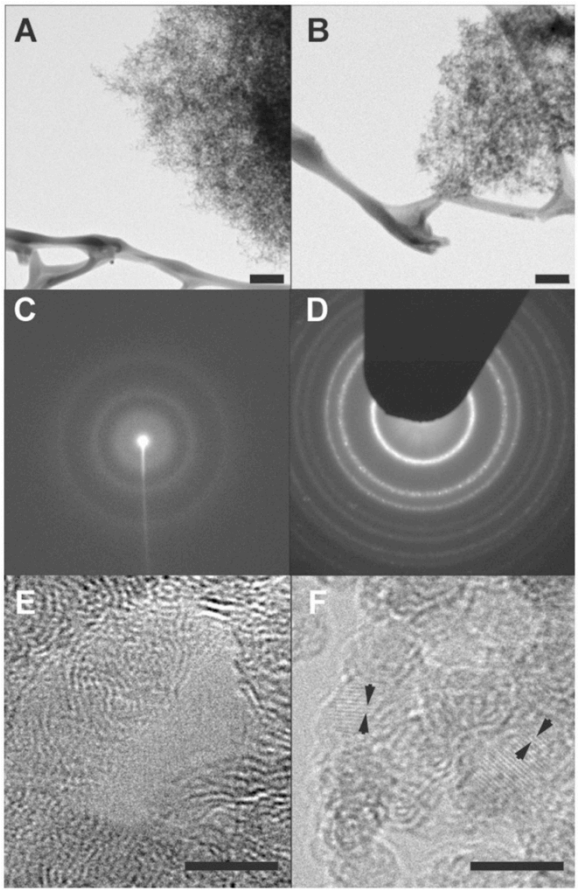

Figure S13. Transmission electron micrographs of amorphous carbon precursor and recovered diamond aerogel. (A and B) Bright-field transmission electron micrographs of amorphous aerogel (A) and recovered aerogel (B). Samples are supported on lacy carbon. Scale bars: 200 nm. (C and D) Corresponding electron diffraction from precursor and recoveredmaterial, respectively. (In D the fundamental beam is blocked.) (E and F) High resolution images of carbon and diamond aerogel microstructure. Nanocrystalline lattice fringes visible in F (arrowheads) correspond to the (111) plane of cubic diamond with a lattice spacing of 2.06 Å. Scale bars: 5 nm. Reproduced by permission from Ref. 10 (Copyright (2011) National Academy of Sciences).

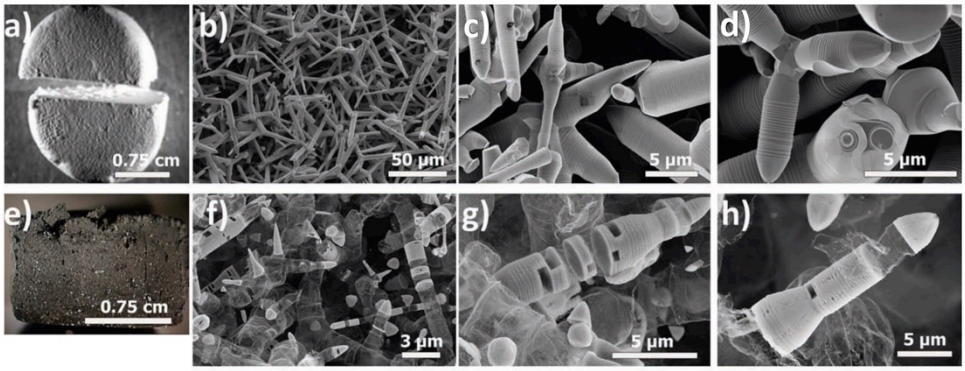

Figure S14. Growth process of Aerographite. a) Photograph of utilized ZnO templates with a volume of 1.77 cm^3. b-d) SEM micrographs showing two examples for the structural variety of ZnO crystal templates, here with a corrugated surface. e) Photograph of an intermediate state of a sample on its way from ZnO to Aerographite. f-h) SEM revealing template removal and formation of carbon layers. Reproduced by permission from Ref. 109 (Wiley and Sons).

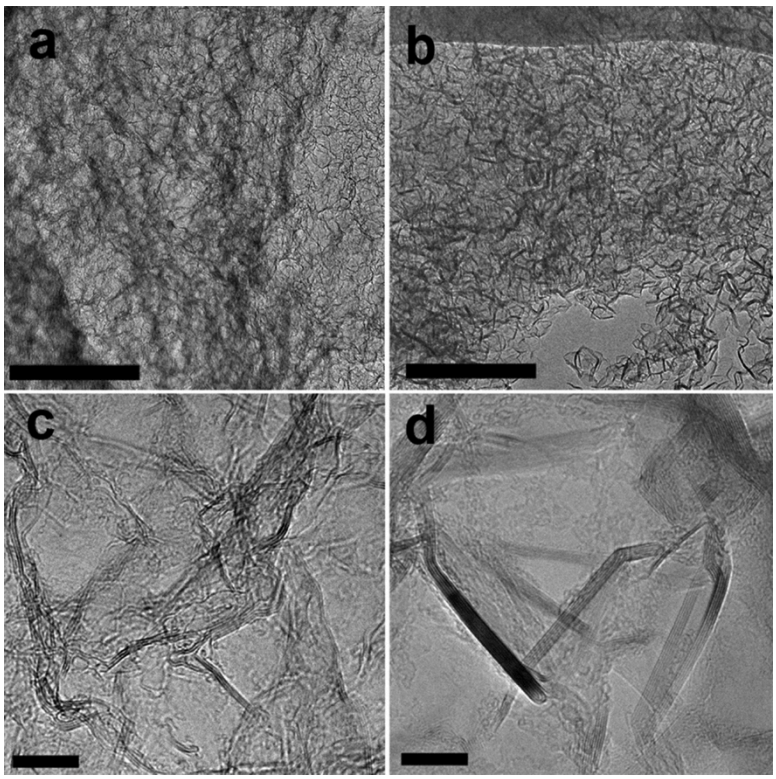

Figure S15. TEM images of original GA (a,c) and converted BN aerogel (b,d). The lower-magnification TEM images (a,b) show that both aerogels are porous with feature sizes of about 30 nm. The higher-magnification TEM images (c,d) show that the aerogels comprise layered structures, indicated by the parallel, dark fringes. Upon conversion to BN, the layered structures become more crystalline with sharp transitions between the facets (d), compared to the more meandering layers

observed in the GAs (c). In addition, the average number of wall for the constituent sheets increases from 2 to 3 in the case of the GAs to 6 to 8 for the BN aerogels. Scale bars are 200 nm (a,c) and 10 nm (c,d). Reproduced by permission from Ref. 17 (American Chemical Society).

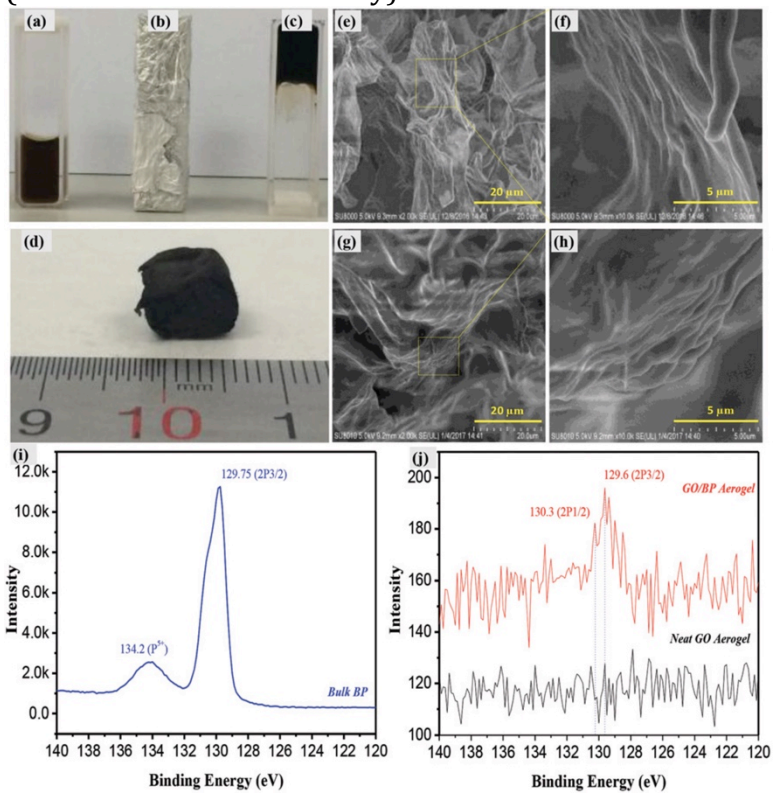

Figure S16. Characterization of 3D GO/BPNF aerogel with 13.4 wt% BP content: (a) homogeneous aqueous solution containing BPNFs, GO nanosheet and D_{400}. (b) Aluminium foil covered reaction vessel. (c) Gelation of GO and BPNFs forming a hydrogel. (d) Macroscopic view of GO/BPNF aerogel after freeze-drying treatment. Field emission scanning electron microscopy (FE-SEM) images of neat GO aerogel (e–f) and GO/BPNF aerogel (g–h), respectively. X-ray photoelectron spectroscopy (XPS) curve of bulk BP (i), neat GO aerogel and GO/BPNF aerogel (j), respectively. Reproduced by permission from Ref. 125 (Royal Society of Chemistry).

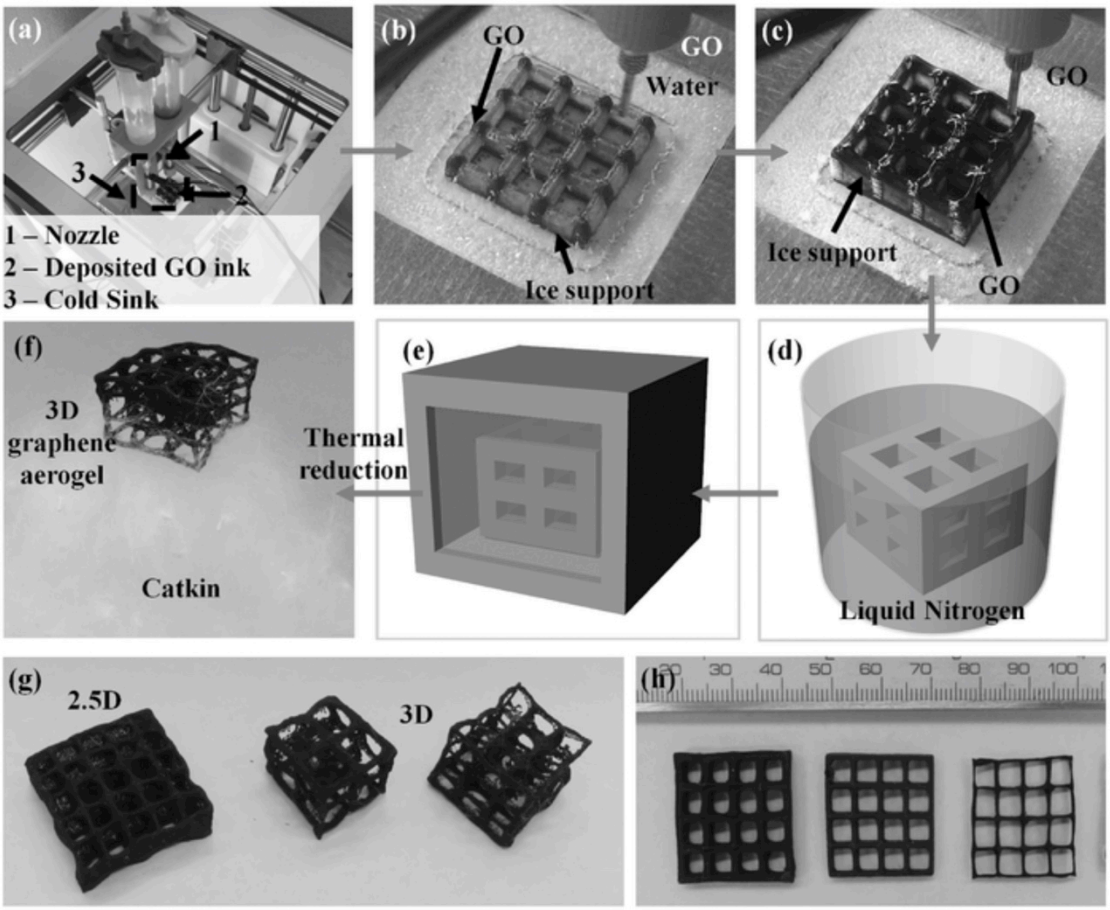

Figure S17. The GA 3D printing process. a) 3D printing setup. b) 3D printing of ice support. c) 3D printing of GO suspension. d) Immersing printed ice structure into liquid nitrogen. e) Freeze drying. f) Thermally reduced to 3D ultralight GA on catkin. g) 3D GA architecture, left: 2.5 structure and right: 3D architecture with overhang structures. h) GAs with various wall thickness. Reproduced by permission from Ref. 148 (Wiley and Sons).